

Data Overlap: A Prerequisite For Disentanglement

Nathan Michlo Steven James Richard Klein
 University of the Witwatersrand
 Johannesburg, South Africa

Nathan.Michlo1@students.wits.ac.za {Steven.James, Richard.Klein}@wits.ac.za

Abstract

Learning disentangled representations with variational autoencoders (VAEs) is often attributed to the regularisation component of the loss. In this work, we highlight the interaction between data and the reconstruction term of the loss as the main contributor to disentanglement in VAEs. We note that standardised benchmark datasets are constructed in a way that is conducive to learning what appear to be disentangled representations. We design an intuitive adversarial dataset that exploits this mechanism to break existing state-of-the-art disentanglement frameworks. Finally, we provide solutions in the form of a modified reconstruction loss suggesting that VAEs are accidental distance learners.

1. Introduction

A fundamental challenge in machine learning is to discover useful representations from high-dimensional data, which can then be used to solve subsequent tasks effectively. Recently, deep learning approaches have showcased the ability of neural networks to extract meaningful features from high-dimensional inputs for tasks ranging from classification [14] to reinforcement learning [22]. While these learned representations have obviated the need for manual feature selection or preprocessing pipelines, they are often not semantically meaningful, which can negatively impact interpretability, fairness [17] and downstream task performance [18].

Prior work has therefore argued that it is desirable to learn a representation that is *disentangled* [1]. While there is no consensus on what constitutes a disentangled representation, it is generally agreed that such a representation should be factorised so that each latent variable corresponds to a single explanatory variable responsible for generating the data [2]. For example, a single image from a video game may be represented by latent variables governing the x and y positions of the player, enemies and collectable items.

A common approach to discovering these seemingly

disentangled representations are variational autoencoders (VAEs) [13], which are trained on unlabelled data to learn a lower-dimensional representation capable of reconstructing the given input. Unfortunately, it has been proven that unsupervised methods cannot reliably learn representations without the introduction of supervision or inductive biases [18]. Fortunately, the recently introduced Ada-GVAE framework has partially overcome this problem by using a weakly supervised signal to discover these underlying factors [19], but there still remains room for improvement.

Interestingly, VAEs do not have an explicit mechanism that encourages the learning of disentangled representations, but it is theorised that this behaviour is related to the regularisation term and the information bottleneck principle, since the decoder minimises errors in the reconstruction process due to random sampling [2, 20, 25]. However, despite this hypothesis, there is still no explicit reason for why the representations learnt by these frameworks should align with generative factors in the data. Nonetheless, these frameworks have been shown to produce disentangled representations (as measured by appropriate metrics [4, 6, 27]) when trained on synthetically generated data such as 3D Shapes [3] and Cars3D [24].

In this paper, we seek to understand why VAEs implicitly learn these disentangled representations by investigating the interaction between the reconstruction loss of the VAE and the input data. We find compelling evidence that disentanglement occurs not because of special algorithmic choices or the regularisation term, but because of the overlap between observations in the datasets themselves. In particular, we find that *these standardised benchmarks are constructed in such a way that they accidentally encourage the models to learn what appear to be disentangled representations*.

The main contributions of this paper are summarised as:

1. We introduce the idea of *visual overlap* and *visual distance* between dataset pairs, measured in terms of the reconstruction loss of VAE frameworks. We show that visual distances in existing datasets naturally correspond to the distances between ground-truth factors, and that VAEs learn these distances. This explains why

the learnt representations appear disentangled.

2. We demonstrate the ineffectiveness of state-of-the-art models by designing a simple adversarial dataset with constant visual distance between elements, over which VAE-based frameworks fail to learn disentangled representations.
3. We propose a solution to the adversarial dataset by simply augmenting the reconstruction loss to increase visual overlap across the dataset such that the framework is able to capture the ground-truth factors. This suggests that VAEs are more akin to distance learners.
4. We contribute *Disent*, a general-purpose modular disentanglement framework built with PyTorch [23], implementing common models, metrics and datasets.¹

2. Related Work

Many publications exist in the areas of VAEs and disentanglement. To the best of our knowledge, the following works are the most applicable to our research, which falls into three broad categories: (i) explanations of disentanglement, (ii) the role of the reconstruction loss in disentanglement, and (iii) problems with disentanglement.

Firstly, Burgess et al. [2] further the understanding of VAEs by relating them to the information bottleneck principle. This explains how random sampling leads to a local minimisation of the reconstruction loss by reorganising the latent space so that points close in pixel space are close in the latent space. Mathieu et al. [20] argue that VAEs do not explicitly encourage disentanglement through their design. Rather, they provide an explanation in terms of the diagonal prior typically used in VAEs combined with random sampling to produce a similar effect to PCA.

Secondly, Hou et al. [10] swap out the reconstruction loss of VAEs for a perceptual loss function, which improves the representations learnt by the model for downstream tasks—one of the benefits of disentanglement. Zietlow et al. [29] extend the analysis by Mathieu et al. [20] for why VAEs disentangle. However, not much focus is placed on the reconstruction loss and its interaction between datasets or their ground-truth factors. Rather, the authors place emphasis on constructing adversarial datasets using a mild transformation to hinder disentanglement performance. The mild transformation is obtained from trained models which achieve poor disentanglement scores.

Finally, Locatello et al. [18] challenge the common assumptions about disentangled representation learning, stating that good representations cannot be reliably learnt with unsupervised methods, unless inductive biases are introduced. Furthermore, Gondal et al. [7] show that often rep-

resentations learnt on synthetic data do not transfer well to real-world data.

3. Background

Assume a dataset $\mathcal{X} = \{\mathbf{x}^{(0)}, \dots, \mathbf{x}^{(n)}\}$ is a set of independent and identically distributed (i.i.d) observations $\mathbf{x} \in \mathbb{R}^N$, generated by some random process involving an unobserved random variable $\mathbf{z} \in \mathbb{R}^D$ of lower dimensionality $D \ll N$. Additionally, the true *prior distribution* $\mathbf{z} \sim p_*(\mathbf{z})$ and true *conditional distribution* $\mathbf{x} \sim p_*(\mathbf{x}|\mathbf{z})$ are unknown. Variational autoencoders (VAEs) aim to learn this generative process. Unlike autoencoders (AEs), which consist of an encoder $f_\phi(\mathbf{x}) = \mathbf{z}$ and decoder $g_\theta(\mathbf{z}) = \hat{\mathbf{x}}$ with weights ϕ and θ , VAEs instead construct a probabilistic encoder by using the output from the encoder or inference model to parameterise approximate posterior distributions $\mathbf{z} \sim q_\phi(\mathbf{z}|\mathbf{x})$. The approximate posterior is then sampled from during training to obtain representations \mathbf{z} , which are then decoded using the generative model to obtain reconstructions $\hat{\mathbf{x}} \sim p_\theta(\mathbf{x}|\mathbf{z})$.

A *factorised Gaussian encoder* [13] is commonly used to model the posterior using a multivariate Gaussian distribution with diagonal covariance $\mathbf{z} \sim \mathcal{N}(\mu_\phi(\mathbf{x}), \sigma_\phi(\mathbf{x}))$, with the prior given by the multivariate normal distribution $p_\theta(\mathbf{z}) = \mathcal{N}(\mathbf{0}, \mathbf{I})$, with a mean of $\mathbf{0}$ and diagonal covariance \mathbf{I} . To enable backpropagation, the reparameterisation trick in Equation (2) is used to sample from the posterior distribution by offsetting the distribution means by scaled noise values.

$$\epsilon \sim \mathcal{N}(\mathbf{0}, \mathbf{I}) \quad (1)$$

$$\mathbf{z} = \mu_\phi(\mathbf{x}) + \sigma_\phi(\mathbf{x}) \odot \epsilon \quad (2)$$

VAEs maximise the evidence lower bound (ELBO) by minimising the loss given by Equation (5). VAE-based approaches often make slight modifications to this loss [4, 8, 10, 11, 15, 19, 28], but the terms of these modified loss functions can usually still be grouped into regularisation and reconstruction components, given by Equations 4 and 3 respectively. The regularisation term affects the representations learnt by the encoder, while the reconstruction term improves the outputs from the decoder. These terms usually contradict in practice, with strong regularisation leading to worse reconstructions but often better disentanglement [2, 8].

$$\mathcal{L}_{\text{rec}}(\mathbf{x}, \hat{\mathbf{x}}) = \mathbb{E}_{q_\phi(\mathbf{z}|\mathbf{x})} [\log p_\theta(\mathbf{x}|\mathbf{z})] \quad (3)$$

$$\mathcal{L}_{\text{reg}}(\mathbf{x}) = -D_{\text{KL}}(q_\phi(\mathbf{z}|\mathbf{x}) \parallel p_\theta(\mathbf{z})) \quad (4)$$

$$\mathcal{L}_{\text{VAE}}(\mathbf{x}, \hat{\mathbf{x}}) = \mathcal{L}_{\text{rec}}(\mathbf{x}, \hat{\mathbf{x}}) + \mathcal{L}_{\text{reg}}(\mathbf{x}) \quad (5)$$

3.1. Random Sampling Reorganises Embeddings

The component within VAE frameworks that encourages disentanglement is the random sampling from the proba-

¹Disent framework: <https://github.com/nmichlo/disent>

bilistic encoder during training. If the distributions parameterised by the encoder overlap sufficiently for different observations, the decoder will often attribute a random sample to an incorrect input (see Figure 1). Thus, a mistake will be made during the decoding process. The reconstruction loss of the VAE encourages the reorganisation of the latent space such that reconstruction mistakes are minimised, with nearby samples in the data space placed close together in the latent space [2].

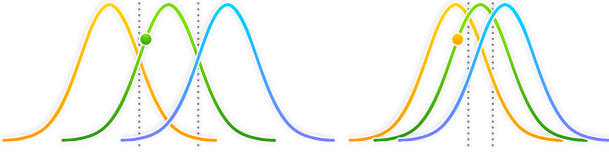


Figure 1. Three nearby distributions in the latent space are presented, each corresponding to different input observations. In each case, the VAE samples from the middle distribution. Left: With weaker regularisation, sampled points are more often attributed to the correct distributions and the decoder correctly reconstructs the observations. Right: With stronger regularisation, sampled points are more often attributed to nearby distributions in the latent space and the decoder makes more mistakes when reconstructing the observation.

The regularisation term in Equation (4) controls the overlap between latent distributions corresponding to different inputs. This is why tuning the strength of the regularisation term in Beta-VAE [8, 19] based frameworks appears to improve disentanglement. Stronger regularisation leads to more latent overlap, making it easier for the decoder to reorganise the embedding space but harder to reconstruct the input. Weaker regularisation lets the system degrade into a lookup table [20]—if few decoding mistakes are made, little reorganisation of the latent space occurs.

The important distinction from literature is that the regularisation term does not directly produce disentangled results. Disentanglement arises from the interaction between the random sampling procedure and the reconstruction term in Equation (3). The regularisation term simply enables this interaction by keeping the probability of making decoding mistakes sufficiently high.

4. Existing Datasets

With an understanding of how VAEs reorganise the latent space, we seek to investigate how the construction of datasets interacts with this process.

Consider the the 3D Shapes dataset [3] in Figure 2, which contains observations of shapes fixed in the centre of the image with progressively changing attributes or factors such as size and colour. If, as humans, we are given unordered observations from a traversal along the size factor of 3D Shapes, it would be easy to order these observa-

tions using a perceived increase or decrease in the size of the shape. We might even say that the shapes in the images overlap by different amounts. We may consider shapes that are closer in size to possess more overlap, and therefore also consider them to be closer together in terms of distance.

It is natural to extend this idea to VAEs constructing orderings over pairs of observations, using both the ground-truth factors as well as how the frameworks themselves perceive the distances between data points.

4.1. Ground-Truth Distance

Synthetic datasets [3, 7, 16, 21, 24] used for benchmarking disentanglement frameworks are all generated from $F \in \mathbb{N}^+$ ground-truth factors of variation. Each factor $i \in [F]$ ² represents some property about the data that can be varied, and has a dimensionality or size of $f_i > 0$ where $f_i \in \mathbb{N}^+$. The set of all factors used for generating the dataset is written as $\mathcal{Y} = [f_1] \times \dots \times [f_F]$. The full dataset is generated from this set of factors using some ground-truth generative process $\mathcal{X} = \{g_*(\mathbf{y}) \mid \mathbf{y} \in \mathcal{Y}\}$. Examples of this generative process are given in Figure 2.

With this construction of synthetic datasets, it is fitting to describe the **ground-truth distances** between observations $\mathbf{x}^{(a)}, \mathbf{x}^{(b)} \in \mathcal{X}$ using the L1 distance between their corresponding ground-truth factors $\mathbf{y}^{(a)}, \mathbf{y}^{(b)} \in \mathcal{Y}$,³ as in Equation (6).

$$d_{gt}(\mathbf{x}^{(a)}, \mathbf{x}^{(b)}) = \|\mathbf{y}^{(a)} - \mathbf{y}^{(b)}\|_1. \quad (6)$$

4.2. Visual Distance

With the idea of ground-truth distances between observations, we need some measure of distance between observations as perceived by VAE frameworks. We derive the *visual distance* between dataset elements from the noisy sampling procedure and the chosen reconstruction loss in a VAE framework.

Let $\mathbf{z}^{(b)} \sim q_\phi(\mathbf{z}|\mathbf{x}^{(a)})$ be a (possibly incorrect) sample from the posterior distribution corresponding to some input element $\mathbf{x}^{(a)} \in \mathcal{X}$. Since the regularisation term encourages latent distributions to overlap, this sample $\mathbf{z}^{(b)}$ may be incorrectly attributed by the decoder to a distribution corresponding to some other element from the dataset $\mathbf{x}^{(b)} \in \mathcal{X}$, with reconstruction $\hat{\mathbf{x}}^{(b)} \approx \mathbf{x}^{(b)}$.

As the VAE objective consisting of the regularisation and reconstruction losses is jointly optimised, the decoder becomes better at reconstructing the inputs. In an ideal scenario, the inputs map to outputs ($\hat{\mathbf{x}} \rightarrow \mathbf{x}$), and reconstructions are samples from our dataset: $\hat{\mathbf{x}} \in \mathcal{X}$. While this is not the case in practice due to the regularisation term, we derive the visual distance in Equation (8) from this assumption that $\hat{\mathbf{x}} \rightarrow \mathbf{x}$. This allows us to directly compare the

²[F] is the bracket notation for the set of natural numbers $\{1, \dots, F\}$.

³For convenience, note that $\mathbf{y}^{(a)} = a$ such that $\mathbf{x}^{(\mathbf{y}^{(a)})} = \mathbf{x}^{(a)}$

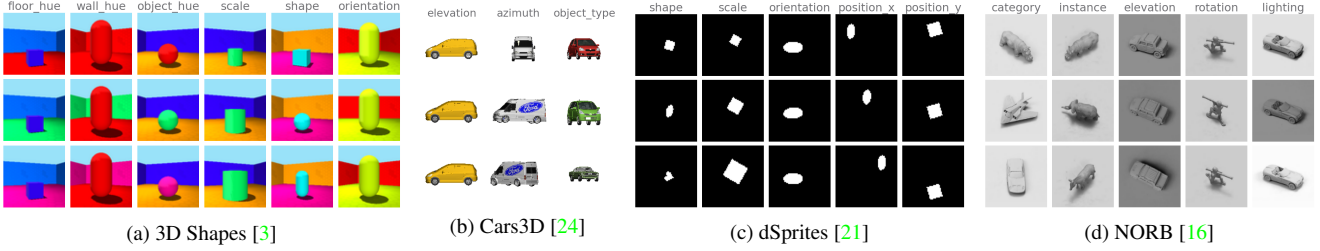


Figure 2. Common existing datasets used to benchmark disentanglement frameworks. These synthetic datasets are generated from ground-truth factors. Columns represent a traversal along a single factor.

elements $\mathbf{x}^{(a)}, \mathbf{x}^{(b)} \in \mathcal{X}$ within a dataset using the reconstruction loss as a distance function:

$$d_{\text{vis}}(\mathbf{x}^{(a)}, \mathbf{x}^{(b)}) = \lim_{\hat{\mathbf{x}} \rightarrow \mathbf{x}} \mathcal{L}_{\text{rec}}(\mathbf{x}^{(a)}, \hat{\mathbf{x}}^{(b)}) \quad (7)$$

$$= \mathcal{L}_{\text{rec}}(\mathbf{x}^{(a)}, \mathbf{x}^{(b)}). \quad (8)$$

The visual distance above depends on the choice of reconstruction loss. The usual choice in literature is the pixel-wise Mean Squared Error (MSE) for data that is assumed to be normally distributed. We assume that MSE loss is used throughout the rest of the paper; however, any analysis should be very similar for other pixel-wise loss functions, such as Binary Cross-Entropy (BCE).

4.3. Visual Distances Correspond To Ground-Truth

In Section 4.1, all the ground-truth factors of a dataset are defined as the set $\mathcal{Y} = [f_1] \times \dots \times [f_F]$. In Equation (10), we now define a *factor traversal* $\mathcal{Y}^{(a,i)} \subset \mathcal{Y}$ as the ordered set of all the coordinates along a factor $i \in [F]$ such that the set passes through a point $\mathbf{y}^{(a)} \in \mathcal{Y}$. The number of elements in the traversal is equal to the size of the chosen factor $|\mathcal{Y}^{(a,i)}| = f_i$, and each element in the traversal generates the same traversal $\forall \mathbf{y}^{(b)} \in \mathcal{Y}^{(a,i)}, \mathcal{Y}^{(a,i)} = \mathcal{Y}^{(b,i)}$.

$$\mathcal{Y}^{(a,i)} = \dots \times \left\{ y_{i-1}^{(a)} \right\} \times [f_i] \times \left\{ y_{i+1}^{(a)} \right\} \times \dots \quad (9)$$

$$= \left\{ (\dots, y_{i-1}^{(a)}, j, y_{i+1}^{(a)}, \dots) \mid \forall j \in [f_i] \right\} \quad (10)$$

We can compute the distance matrices $\tilde{D}^{(a,i)} \in \mathbb{R}^{f_i \times f_i}$ for some distance function d between pairwise elements along a factor traversal $\mathcal{Y}^{(a,i)}$ using Equation (11).

$$\tilde{D}^{(a,i)} = \left(d(\mathbf{x}^{(u)}, \mathbf{x}^{(v)}) \right) \in \mathbb{R}^{f_i \times f_i} \quad \forall u, v \in \mathcal{Y}^{(a,i)} \quad (11)$$

To characterise the factors within our dataset, we compute the average distance matrices $D^{(i)} = \mathbb{E}_{a \in \mathcal{Y}}[\tilde{D}^{(a,i)}]$ for each factor $i \in [F]$. We plot these results in Figure 3 for the ground-truth distance d_{gt} and visual distance d_{vis} . It is immediately obvious from these plots that the ground-truth and visual distances as perceived by a VAE correspond. When a VAE reorganises the embedding space, it is likely

to discover structures that are similar to the ground-truth factors and distances themselves.

We further examine this in Figure 4, where we compute distance matrices over a trained Beta-VAE at various levels of the network, including the representation layer and reconstructions. At each level of the VAE, the learnt distances all correspond to the original visual distances already present within the dataset due to the chosen loss.

Since a VAE with a factorised Gaussian prior is known to be rotationally invariant [20], the same distances between the means μ of latent distributions can be learnt for any arbitrary rotation of the latent space. Our results in Figures 3 and 4 provide empirical evidence that VAEs mimic the distances already present in the dataset according to the reconstruction loss. This suggests that VAEs disentangle by accident, since ground-truth factors naturally correspond with distances in the dataset. If these visual distances were to change such that they do not correspond to the ground-truth distances, VAEs might not be able to learn meaningful representations. This is highlighted by the fact that VAEs are already known to perform poorly on real-world data [7]. Real-world data often has noise, imperfections or backgrounds which may mask the distances and factors that we care about.

4.4. Identifying Factor Importance

A factor in a dataset is considered more important if a VAE prefers to learn it before another factor. Burgess et al. [2] identify this order of importance through a slow increase of the information capacity of VAEs during training. We note that simply by looking at the average visual distance between observations along factor traversals, this ordering can be determined. Factors with a greater average distance will minimise the error in the reconstruction loss due to random sampling the most when learnt first. These factors (or components thereof) will thus generally be preferred.

To compute the average visual distance along a factor f , we sample a ground-truth coordinate vector $\mathbf{y}^{(a)} \in \mathcal{Y}$ and then another random different coordinate vector $\mathbf{y}^{(b)} \in \mathcal{Y}^{(a,i)}$ over the traversal for factor f passing through $\mathbf{y}^{(a)}$. Note that $\mathbf{y}^{(a)} \neq \mathbf{y}^{(b)}$. Then, we com-

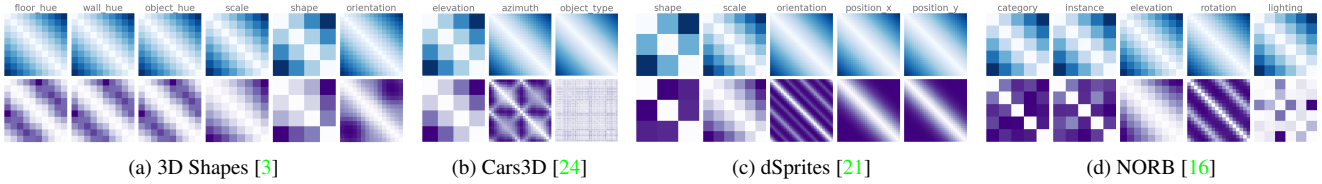


Figure 3. Distances in the ground-truth factor space naturally correspond to distances in the data space for current synthetic datasets. Top Row: Average Manhattan distance matrices over factor traversals. Bottom Row: Average pixel-wise visual distance matrices (MSE) over observations from the same factor traversals. Columns: Different ground-truth factors within each dataset.

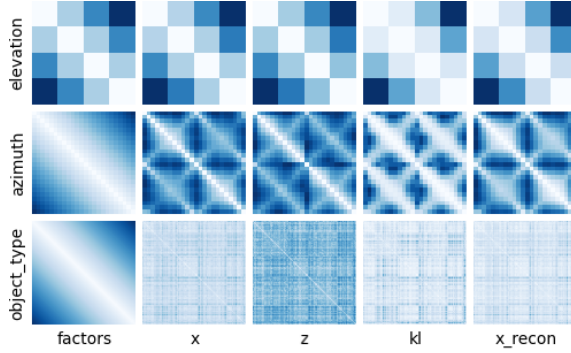


Figure 4. Beta-VAEs learn similar distances between observations at each level of the network depending on the reconstruction loss. Rows: Different factors of the Cars3D dataset (Top to bottom: elevation, azimuth, car type), Columns: Different sources of distance matrices computed over factor traversals (Left to right: ground-truth distances, visual distances between observations, L2 distances over latent distribution means, KL divergences between latent distributions, visual distances between reconstructions.)

pute the visual distance between the corresponding observations $d_{\text{vis}}(\mathbf{x}^{(a)}, \mathbf{x}^{(b)})$. We repeat this process to compute the expected visual distance along factor traversals, given by Equation (12).

$$d_i = \mathbb{E}_{a \in \mathcal{Y}, b \in \mathcal{Y}^{(a,i)}, a \neq b} [d_{\text{vis}}(\mathbf{x}^{(a)}, \mathbf{x}^{(b)})] \quad (12)$$

We determine the factor importance for dSprites as: $d_{\mathbf{x}a} \approx 0.058$ and $d_y \approx 0.057$ position, then $d_{\text{scale}} \approx 0.025$, then $d_{\text{shape}} \approx 0.022$, and finally $d_{\text{orientation}} \approx 0.017$. This aligns with the order determined by Burgess et al. [2]. Computing estimates over an entire dataset can be intractable—for our estimates, we sample at least 50000 pairs per factor.

Additionally, we compute the average visual distance between any random pairs in the datasets (see Equation (13)) and find that the average distance is higher. For dSprites specifically, we have $d_{\text{ran}} \approx 0.075$. This suggests that the ground-truth factors correspond to axes in the data that minimise the reconstruction loss and is further evidence as to why VAEs appear to learn disentangled results.

$$d_{\text{ran}} = \mathbb{E}_{a \in \mathcal{Y}, b \in \mathcal{Y}, a \neq b} [d_{\text{vis}}(\mathbf{x}^{(a)}, \mathbf{x}^{(b)})] \quad (13)$$

5. Adversarial Dataset

In the previous section, we highlighted the striking similarity between the ground-truth distances and the visual distances between observations in a dataset. This suggests that disentanglement occurs because VAEs accidentally correspond to ground-truth distances when the latent space is re-organised to capture visual distances in the data space.

Consider an example where a single chess piece moves across a chess board and there are no smooth transitions between grid points, since the piece is only valid when placed in the middle of squares.

We describe such a dataset as having constant overlap or constant visual distance. It is also adversarial, because it is impossible to order observations using pairwise distance comparisons. It may be tempting to think that a harder case to solve is if the visual distances simply do not correspond to ground-truth distances; however, an (incorrect) ordering can still be found. Existing datasets such as Cars3D (see Figure 3) already satisfy this property, which may explain the generally worse disentanglement performance compared to other datasets.

Formally, we say that a dataset has constant overlap when the pairwise distances over factor traversals are all equal. Let $i \in [F]$ be a factor and $\mathbf{y}^{(a)} \in \mathcal{Y}$ be ground-truth coordinate vector. Then, for all elements over the factor traversal $\forall \mathbf{y}^{(b)} \in \mathcal{Y}^{(a,i)} / \mathbf{y}^{(a)}$, the corresponding visual overlap is constant such that $d_{\text{vis}}(\mathbf{x}^{(a)}, \mathbf{x}^{(b)}) = C_f$ with $C_f \in \mathbb{R}$ and $C_f > 0$. Along factor traversals in such a dataset, no distinct ordering of elements can be found when a VAE tries to minimise the sampling error over the reconstruction loss. Going forward, we only consider the case where $\forall f \in [F]$, $C_f = C$ for some $C > 0$.

5.1. XYSquares Dataset

Taking inspiration from the chess piece example, we design a synthetic adversarial dataset called *XYSquares*, illustrated by Figure 5, to exploit the VAE weakness of constant overlap when traversing factors. The dataset consists of three squares, where each square is 8×8 pixels in size. With an observation size of 64×64 pixels, this leaves 8 grid positions along each x and y axis while avoiding any

pixel-wise overlap. The three squares are each assigned a colour according to R (1, 0, 0), G (0, 1, 0) and B (0, 0, 1) to avoid any channel-wise overlap. With 6 ground-truth factors (three squares moving along two axes), each with 8 possible values, this gives a total dataset size of $8^6 = 262144$ observations.

We validate the design of the dataset in Figure 7 against other commonly used datasets by comparing the visual distance between pairs of observations along factors. The results in Figure 3 show that when randomly sampling differing pairs along factor traversals, our dataset maintains constant pixel-wise distance values.

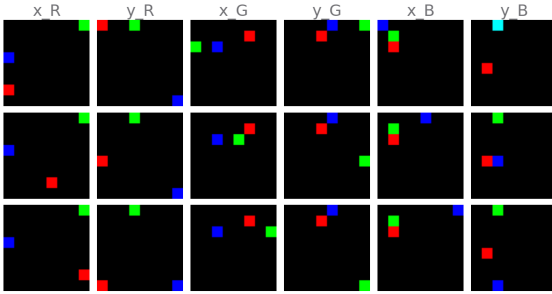


Figure 5. Columns represent ground-truth factor traversals over our adversarial XYSquares dataset. The dataset consists of 3 squares, each of which can move along 8 distinct x and y grid positions, for a total of 6 ground-truth factors and $8^6 = 262144$ observations. A pixel-wise distance measure has constant values between any two differing observations along a factor traversal.

5.2. Experimental Setup

We now investigate the performance of VAEs on our new dataset. In particular, we use the unsupervised Beta-VAE [8] and the state-of-the-art weakly supervised Ada-GVAE [19]. The Beta-VAE scales the VAE regularisation term with a coefficient $\beta > 0$, while the Ada-GVAE encourages axis alignment and shared latent variables between pairs of observations. This is achieved by averaging together latent distributions between observation pairs that are estimated to remain unchanged when the KL divergence is below some threshold. We note that if the weakly supervised Ada-GVAE performs poorly, then it is highly likely that another unsupervised method will also perform poorly.

We use the same standardised Adam [12] optimizer and convolutional neural architecture as Burgess et al. [2], with fully connected networks around the bottleneck layer.

To evaluate disentangled representations, we use the MIG [4] (Mutual Information Gap) and DCI Disentanglement [6] scores. MIG measures the mutual information between the highest and second highest latent units for each factor, and DCI Disentanglement measures how much each latent unit captures a ground-truth factor using a predictive

model.

Finally, we perform an extensive hyper-parameter grid search on existing frameworks and datasets before running our own experiments. Hyperparameters include the learning rate, size of the latent dimension, training steps, batch size and β values. See the supplementary material for further details on all experiments conducted throughout the remainder of the paper.

5.3. Adversarial Experiments

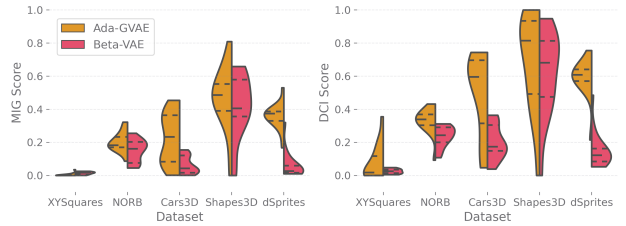


Figure 6. MIG score (Left) and DCI Disentanglement score (Right) for the weakly-supervised Ada-GVAE (Left half of densities) and Beta-VAE (Right half of densities) on commonly used datasets compared to our adversarial dataset (x axis) with constant pixel-wise visual overlap. Our adversarial dataset hurts the disentanglement performance significantly. Quartiles are marked with horizontal lines. Multiple runs are performed over a sweep of β values and latent dimension sizes. See the supplementary material for further details.

The results in Figure 6 show that the disentanglement performance over XYSquares is extremely poor compared to existing datasets, even with the state-of-the-art Ada-GVAE. We are not concerned with the distribution of scores, rather the maximum score obtained for each model and dataset. This validates our adversarial dataset hypothesis in Section 5. Not only is the disentanglement performance poor, but much smaller values for β are needed when tuning the regularisation loss.

5.4. Varying Levels of Overlap

We have examined the effect of training on existing datasets with significant amounts of overlap, as well as our own adversarial dataset with constant overlap. However, we have not investigated increasing levels of overlap in datasets. To do so, we modify XYSquares by decreasing the spacing between grid points while keeping the number of grid points constant along each factor, such that the size of the dataset remains the same at $8^6 = 262144$ observations.

The original adversarial dataset with a spacing of 8 has a constant distance value of $d_{\text{vis}}(\mathbf{x}^{(a)}, \mathbf{x}^{(b)}) = C_8$. As the spacing s decreases from $8 \rightarrow 1$ over the datasets, the probability increases that any two observations re-sampled along

a single factor traversal overlap $p(d_{\text{vis}}(\mathbf{x}^{(a)}, \mathbf{x}^{(b)}) < C_8)$ and should thus be placed closer together in the latent space. More overlap leads to more unique distance values which in turn allows for easier ordering of data points. We visualise this concept using ground-truth and visual distance matrices in Figure 7.

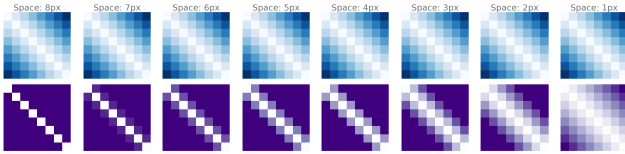


Figure 7. Top Row: Manhattan ground-truth distance matrices over factor traversals. Bottom Row: Pixel-wise visual distance matrices between observations over factor traversals. Left to Right: The spacing between grid-points of XYSquares decreases from 8px to 1px introducing more overlap into the data space. More overlap leads to higher probability of being able to induce an ordering along a factor traversal. In XYSquares, each ground-truth factor has the same characteristics.

We verify our statements through the experimental results in Figure 8, where the Beta-VAE and Ada-GVAE are trained on these datasets. As the spacing decreases and overlap is introduced, the disentanglement performance improves, since it is easier for a VAE to introduce an ordering over representations. Even for the XYSquares dataset with 1 pixel of overlap between grid points, an ordering of elements along factor traversals can be induced. However, the probability of a VAE encountering these scenarios in the latent space due to random sampling is low, and thus it is still not always easy for the model to learn disentangled representations over such a dataset.

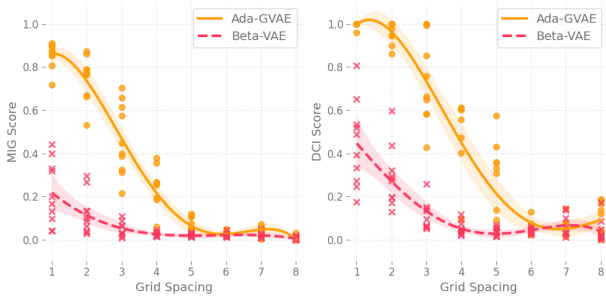


Figure 8. Regression plots over increasing spacing of the XYSquares dataset versus MIG score (Left) and DCI Disentanglement score (Right). As the weakly-supervised Ada-GVAE (solid lines) and Beta-VAE (dashed lines) are trained with these decreasing (left to right) levels of overlap, their disentanglement performance worsens. Each experiment is repeated 5 times with previously tuned hyper-parameters. See the supplementary material for further experimental details.

6. Introducing Overlap

The previous section focused on increasing overlap by changing the underlying dataset; however, this still does not solve the case for the original constant-overlap XYSquares dataset. Throughout this paper, we have provided evidence that VAEs disentangle based on their reconstruction loss. To solve this problem, we need to carefully choose a loss function that introduces appropriate overlap such that when visual distances are measured, they also correspond to ground-truth distances.

The new loss function we choose cannot be a pixel-wise approach, as this does not capture the distances due to the spatial nature of the XYSquares dataset. For the sake of simplicity, we convert the existing pixel-wise loss function into a spatially aware loss function by introducing a differentiable augmentation to its inputs. An appropriate augment for our dataset is a channel-wise box blur. The problem, however, is that the decoder needs to be able to reconstruct the data, and so purely replacing the pixel-wise loss with the augmented spatially-aware version may not succeed. Rather, in Equation (14), we append the augmented term to the existing loss and scale it by a constant $\alpha > 0$.

$$\begin{aligned} \mathcal{L}_{\text{Overlap}}(\mathbf{x}, \hat{\mathbf{x}}) = & \mathcal{L}_{\text{rec}}(\mathbf{x}, \hat{\mathbf{x}}) \\ & + \alpha \mathcal{L}_{\text{rec}}(\text{blur}(\mathbf{x}), \text{blur}(\hat{\mathbf{x}})) \end{aligned} \quad (14)$$

6.1. Augmented Loss Experiments

The loss function we choose uses a channel-wise box blur with a radius of 31, for a total kernel size of 63×63 . We implement large filters efficiently using the Fast Fourier Transform. The size of the filter ensures that if two observations have active pixels on opposite sides of the images, then overlap will still be introduced between them. We set $\alpha = 63^2$ —while this appears large, a box blur kernel is normalised so that the sum of all its values is 1. We accordingly update our visual distance measure and evaluate the distances within the XYSquares dataset for each factor in Figure 9 by training tuned Beta-VAEs. It is interesting to note that in the case of the pixel-wise loss over the adversarial dataset, a small subset of observations are placed closer together in the latent space. We hypothesise this is due to learning biases introduced by the neural networks themselves, since this is not captured by the various loss functions. We leave an investigation of this to future work.

Finally, we compare the performance of the spatially-aware loss function in Figure 10 to the original pixel-wise loss. Our new loss significantly improves the disentanglement performance over the adversarial dataset. This is because it allows our models to capture visual distances between observations that align with the ground-truth factors.

While our choice of loss may not be optimal for disentanglement of these specific x and y factors from our adversarial dataset, disentanglement results are impressive. This

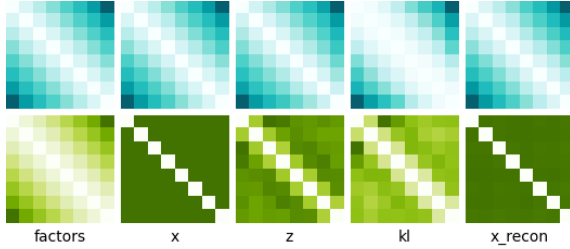


Figure 9. Similar to Figure 4, Beta-VAEs learn similar distances between observations at each level of the network depending on the reconstruction loss. This suggests that VAEs are approximate distance learners with respect to the reconstruction loss. Top row: box blur augmented MSE. Bottom row: pixel-wise MSE loss. Columns: Different sources of distance matrices computed over factor traversals within a VAE (Left to right: ground-truth distances, visual distances between observations, L2 distances over latent distribution means, KL divergences between latent distributions, visual distances between reconstructions.)

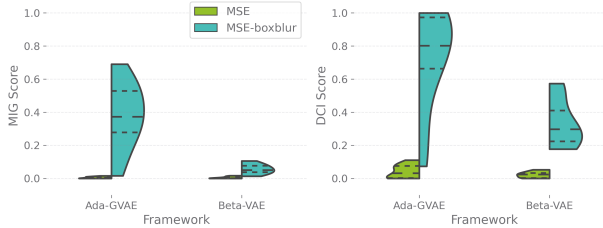


Figure 10. MIG and DCI scores for Ada-GVAE and Beta-VAE using the MSE loss and our modified loss function. Introducing a spatially aware loss function allows us to capture ground-truth distances between observations and allows the models to disentangle the adversarial XYsquares dataset.

is important, because it provides the intuition that changing the loss function can affect the ability of VAE frameworks to learn disentangled representations. We leave the identification and learning of optimal loss functions for targeted disentanglement to future work.

7. Considerations for Disentanglement Research

VAEs reorganise the latent space to minimise the reconstruction error due to random sampling. We argue that this should not be considered disentanglement. Rather, as Figures 4 and 9 illustrate, it is closer to distance learning [9, 26] and only approximates disentanglement.

We also observe that adjusting the reconstruction loss changes the representations learnt by affecting overlap and thus disentanglement. In practice, careful tuning and choice of the loss function may be needed to capture different ground-truth factors. However, changing the loss to capture one factor may conflict with the models ability to learn

another factor.

Furthermore, learning ground-truth factors is an inherently subjective process. There are often multiple ways to represent these factors within datasets and these choices may change depending on the task at hand or the requirements of the researcher. For example, factors may be decomposed into multiple sub-factors or merged into single parent factors. Disentanglement metrics that cannot capture these relationships may incorrectly attribute worse scores. We illustrate this in Figure 11, where VAEs often prefer to learn the “azimuth” or “object type” factors using multiple latent variables when trained on Cars3D.

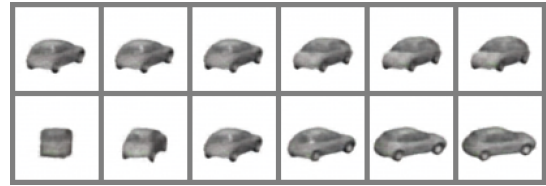


Figure 11. Models prefer to learn the “azimuth” factor of the Cars3D dataset with two latent variables: One latent variable that controls a partial rotation (bottom row) and one latent variable that flips the car around (top row). This corresponds to our distance plots in Figure 3, which are clearly segmented. Models additionally prefer to learn the large “object type” factor as multiple sub-factors, which may include colour of the car, shape of the car, height of the car, etc.

8. Conclusion

In this paper, we demonstrated that there are fundamental characteristics of existing datasets that encourage VAEs to learn disentangled representations. Based on the observation that the visual distances between pairs of data points correspond to their ground-truth distances, and that VAEs inherently learn these distances, we constructed a simple dataset for which state-of-the-art models were unable to disentangle. Finally, we proposed a modification to the VAE reconstruction loss that enabled successful learning of disentangled representations by changing distances in the data space.

Our results highlight issues in current representation learning approaches. If we ever hope to apply these models to real world data, then overlap in datasets *cannot* be a prerequisite—more advanced methods are required that can uncover meaning within the data.

References

- [1] Yoshua Bengio, Aaron Courville, and Pascal Vincent. Representation learning: A review and new perspectives. *IEEE Transactions on Pattern Analysis and Machine Intelligence*, 35(8):1798–1828, 2013. 1

[2] Christopher Burgess, Irina Higgins, Arka Pal, Loic Matthey, Nick Watters, Guillaume Desjardins, and Alexander Lerchner. Understanding disentangling in β -VAE. In *Workshop on Learning Disentangled Representations at the 31st Conference on Neural Information Processing Systems*, 2017. 1, 2, 3, 4, 5, 6, 11, 12

[3] Christopher Burgess and Hyunjik Kim. 3D shapes dataset. <https://github.com/deepmind/3dshapes-dataset/>, 2018. 1, 3, 4, 5, 10, 13

[4] Ricky Chen, Xuechen Li, Roger Grosse, and David Duvenaud. Isolating sources of disentanglement in variational autoencoders. In *Advances in Neural Information Processing Systems*, pages 2615–2625, 2018. 1, 2, 6

[5] Andrea Dittadi, Frederik Träuble, Francesco Locatello, Manuel Wuthrich, Vaibhav Agrawal, Ole Winther, Stefan Bauer, and Bernhard Schölkopf. On the transfer of disentangled representations in realistic settings. In *International Conference on Learning Representations*, 2021. 10

[6] Cian Eastwood and Christopher Williams. A framework for the quantitative evaluation of disentangled representations. In *International Conference on Learning Representations*, 2018. 1, 6

[7] Muhammad Waleed Gondal, Manuel Wuthrich, Djordje Miladinovic, Francesco Locatello, Martin Breidt, Valentin Volchkov, Joel Akpo, Olivier Bachem, Bernhard Schölkopf, and Stefan Bauer. On the transfer of inductive bias from simulation to the real world: a new disentanglement dataset. *Advances in Neural Information Processing Systems*, 32:15740–15751, 2019. 2, 3, 4

[8] Irina Higgins, Loic Matthey, Arka Pal, Christopher Burgess, Xavier Glorot, Matthew Botvinick, Shakir Mohamed, and Alexander Lerchner. beta-vae: Learning basic visual concepts with a constrained variational framework. 2016. 2, 3, 6, 10

[9] Elad Hoffer and Nir Ailon. Deep metric learning using triplet network. In *International workshop on similarity-based pattern recognition*, pages 84–92. Springer, 2015. 8

[10] Xianxu Hou, Linlin Shen, Ke Sun, and Guoping Qiu. Deep feature consistent variational autoencoder. In *2017 IEEE Winter Conference on Applications of Computer Vision*, pages 1133–1141. IEEE, 2017. 2

[11] Hyunjik Kim and Andriy Mnih. Disentangling by factorising. In *International Conference on Machine Learning*, pages 2649–2658. PMLR, 2018. 2, 10

[12] Diederik Kingma and Jimmy Ba. Adam: A method for stochastic optimization. In *International Conference on Learning Representations*, 2015. 6, 10

[13] Diederik Kingma and Max Welling. Auto-encoding variational bayes. In *International Conference on Learning Representations*, 2014. 1, 2

[14] Alex Krizhevsky, Ilya Sutskever, and Geoffrey Hinton. Imagenet classification with deep convolutional neural networks. *Advances in Neural Information Processing Systems*, 25:1097–1105, 2012. 1

[15] Abhishek Kumar, Prasanna Sattigeri, and Avinash Balakrishnan. Variational inference of disentangled latent concepts from unlabeled observations. In *International Conference on Learning Representations*, 2018. 2

[16] Yann LeCun, Fu Jie Huang, and Leon Bottou. Learning methods for generic object recognition with invariance to pose and lighting. In *IEEE Computer Society Conference on Computer Vision and Pattern Recognition*, 2004. 3, 4, 5, 10, 13

[17] Francesco Locatello, Gabriele Abbati, Thomas Rainforth, Stefan Bauer, Bernhard Schölkopf, and Olivier Bachem. On the fairness of disentangled representations. In *Advances in Neural Information Processing Systems*, pages 14584–14597, 2019. 1

[18] Francesco Locatello, Stefan Bauer, Mario Lucic, Gunnar Raetsch, Sylvain Gelly, Bernhard Schölkopf, and Olivier Bachem. Challenging common assumptions in the unsupervised learning of disentangled representations. In *International Conference on Machine Learning*, pages 4114–4124. PMLR, 2019. 1, 2, 10

[19] Francesco Locatello, Ben Poole, Gunnar Rätsch, Bernhard Schölkopf, Olivier Bachem, and Michael Tschannen. Weakly-supervised disentanglement without compromises. In *International Conference on Machine Learning*, pages 6348–6359. PMLR, 2020. 1, 2, 3, 6, 10

[20] Emile Mathieu, Tom Rainforth, Nana Siddharth, and Yee Whye Teh. Disentangling disentanglement in variational autoencoders. In *International Conference on Machine Learning*, pages 4402–4412. PMLR, 2019. 1, 2, 3, 4

[21] Loic Matthey, Irina Higgins, Demis Hassabis, and Alexander Lerchner. dSprites: Disentanglement testing sprites dataset. <https://github.com/deepmind/dsprites-dataset/>, 2017. 3, 4, 5, 10, 11, 13

[22] Volodymyr Mnih, Koray Kavukcuoglu, David Silver, Andrei A Rusu, Joel Veness, Marc G Bellemare, Alex Graves, Martin Riedmiller, Andreas K Fidjeland, Georg Ostrovski, et al. Human-level control through deep reinforcement learning. *Nature*, 518(7540):529–533, 2015. 1

[23] Adam Paszke, Sam Gross, Soumith Chintala, Gregory Chanan, Edward Yang, Zachary DeVito, Zeming Lin, Alban Desmaison, Luca Antiga, and Adam Lerer. Automatic differentiation in PyTorch. 2017. 2

[24] Scott Reed, Yi Zhang, Yuting Zhang, and Honglak Lee. Deep visual analogy-making. *Advances in Neural Information Processing Systems*, 28:1252–1260, 2015. 1, 3, 4, 5, 10, 13

[25] Michal Rolinek, Dominik Zietlow, and Georg Martius. Variational autoencoders pursue PCA directions (by accident). In *Proceedings of the IEEE/CVF Conference on Computer Vision and Pattern Recognition*, pages 12406–12415, 2019. 1

[26] Liu Yang and Rong Jin. Distance metric learning: A comprehensive survey. *Michigan State Universiy*, 2(2):4, 2006. 8

[27] Julian Zaidi, Jonathan Boilard, Ghyslain Gagnon, and Marc-André Carboneau. Measuring disentanglement: A review of metrics. *arXiv preprint arXiv:2012.09276*, 2020. 1

[28] Shengjia Zhao, Jiaming Song, and Stefano Ermon. InfoVAE: Information maximizing variational autoencoders. *arXiv preprint arXiv:1706.02262*, 2017. 2

[29] Dominik Zietlow, Michal Rolinek, and Georg Martius. Demystifying inductive biases for β -VAE based architectures. *arXiv preprint arXiv:2102.06822*, 2021. 2

A. Implementation Details

In this section, we describe our various implementation details of the Beta-VAE [8] and Ada-GVAE [19] frameworks, as well as the handling and standardisation of the different ground-truth datasets.

A.1. Beta Normalisation

For general consistency across datasets with different numbers of channels and models with different numbers of latent units, we implement beta normalisation as described by Higgins et al. [8].

Instead of taking the sum over the KL divergence in the regularisation term and the sum over elements in the reconstruction term of the VAE loss, we instead compute the means over elements in both terms and adjust the β value accordingly.

A.2. Symmetric KL

The original Ada-GVAE implementation uses the asymmetric KL divergence $D_{\text{KL}}(p \parallel q)$ as the distance function between the corresponding latent units of observation pairs. The Ada-GVAE uses this distance to estimate which of these latent units should be averaged together.

We instead follow the approach of Dittadi et al. [5] and use the symmetric KL divergence to compute these distances between latent units, improving the averaging procedure and computation of the threshold. The symmetric KL divergence is defined in Equation (15).

$$\tilde{D}_{\text{KL}}(p, q) = \frac{1}{2}D_{\text{KL}}(p \parallel q) + \frac{1}{2}D_{\text{KL}}(q \parallel p) \quad (15)$$

A.3. Sampling Ada-GVAE Pairs

The Ada-GVAE [19] framework introduces weak supervision by sampling pairs of observations such that there are always $k \in [1, F]$ differing factors between them. We use the weaker but more realistic case where k is sampled uniformly randomly for each pair as described in the original paper.

A.4. Dataset Standardisation

For improved consistency and training performance, dataset observations are standardised. We first resize the observations to a width and height of 64×64 pixels using bilinear filtering. Then the observations are normalised such that on average each channel of the image has a mean of 0 and a standard deviation of 1. Normalisation constants for each channel are precomputed across the entire dataset and are given in Table 1.

B. Experiment Details

In this section, we give further details on the experiments conducted throughout the paper and their chosen hyper-

Dataset	Mean	Std
Cars3D [24]	R : 0.897667614997663	0.225031955315030
	G : 0.889165802006751	0.239946127898126
	B : 0.885147515814868	0.247921063196844
3D Shapes [3]	R : 0.502584966788819	0.294081404355556
	G : 0.578759756608967	0.344397908751721
	B : 0.603449973185958	0.366168598152475
Small NORB [16]	0.752091840108860	0.095638790168273
dSprites [21]	0.042494423521890	0.195166458806261
XYsquares	R : 0.015625	0.124034734589209
	G : 0.015625	0.124034734589209
	B : 0.015625	0.124034734589209

Table 1. Precomputed channel-wise normalisation constants for datasets, assuming the input data is in the range $[0, 1]$.

parameters. For easier comparison with prior work, we use similar hyper-parameters, optimiser and model choices to Higgins et al. [8], Kim and Mnih [11], Locatello et al. [18].

B.1. Model Architecture

We use similar convolutional encoder and decoder models as Higgins et al. [8], given in Table 2. The Gaussian encoder parameterises the mean and log variance of each latent distribution. The decoder uses the Gaussian derived Mean Squared Error (MSE) as the loss function. The number of input channels the encoder receives and the number of output channels the decoder produces depends on the dataset the model is trained on, this is either 1 or 3 channels.

Encoder	Decoder
Input {1 or 3}x64x64	Input {9 or 25}
Conv. 32x4x4 (<i>stride 2</i> , ReLU)	Linear 256 (ReLU)
Conv. 32x4x4 (<i>stride 2</i> , ReLU)	Linear 1024 (<i>reshape 64x4x4</i> , ReLU)
Conv. 64x4x4 (<i>stride 2</i> , ReLU)	Upconv. 64x4x4 (<i>stride 2</i> , ReLU)
Conv. 64x4x4 (<i>stride 2</i> , ReLU)	Upconv. 32x4x4 (<i>stride 2</i> , ReLU)
Linear 256 (ReLU)	Upconv. 32x4x4 (<i>stride 2</i> , ReLU)
2x Linear {9 or 25}	Upconv. {1 or 3}x4x4 (<i>stride 2</i>)

Table 2. Encoder and decoder architectures based on Locatello et al. [18]. Model inputs and outputs change based on the number of channels in the dataset. Model latent units depend on the experiment hyper-parameters.

B.2. Optimiser and Batch Size

Models are trained using the Adam [12] optimiser with a learning rate of 10^{-3} . A batch size of 256 is used in the case of the Beta-VAE [8]. In the case of the Ada-GVAE [19], 256 observation pairs are used per batch.

B.3. Experiment Sweeps

Experiment plots are produced over hyper-parameter sweeps. Grid search values are given in Table 3.

C. Factor Importance Plots

In Section 4.4, we relate our work to Burgess et al. [2] by estimating the importance of different factors over the dSprites [21] dataset using the reconstruction loss (MSE) as the visual distance function between observation pairs. We compute and list the order of importance of factors from the remaining datasets in Table 4.

We can visualise the distribution of distances along factor traversals using cumulative frequency plots as in Figure 12. It is interesting to note the distinct shift in features over the adversarial dataset.

Experiment	Total	Hyper-Parameters
5.3. Adversarial Experiments (Figure 6)	$8 \times 2 \times 2 \times 5$ = 160 $\times 1$ repeats = 160	train steps = 115200 beta (β) $\in \{0.000316, 0.001, 0.00316, 0.01, 0.0316, 0.1, 0.316, 1.0\}$ framework $\in \{\text{Beta-VAE, Ada-G-VAE}\}$ latents (D) $\in \{9, 25\}$ dataset $\in \{\text{dSprites, 3D Shapes, Cars3D, Small NORB, XYsquares}\}$
5.4. Varying Levels of Overlap (Figure 8)	$2 \times 2 \times 8$ = 32 $\times 5$ repeats = 160	train steps = 57600 beta (β) $\in \{0.001, 0.00316\}$ framework $\in \{\text{Beta-VAE, Ada-G-VAE}\}$ latents (D) = 9 dataset = XYsquares grid spacing $\in \{8, 7, 6, 5, 4, 3, 2, 1\}$
6.1. Augmented Loss Experiments (Figure 10)	$2 \times 2 \times 2$ = 8 $\times 5$ repeats = 40	train steps = 57600 beta (β) $\in \{0.0001, 0.0316\}$ framework $\in \{\text{Beta-VAE, Ada-G-VAE}\}$ latents (D) = 25 dataset = XYsquares recon. loss $\in \{\text{MSE, BoxBlurMSE}\}$ box blur radius = 31 (63x63 in size) box blur weight = $63^2 = 3969$

Table 3. Grid search hyper-parameters used for the different experiments throughout this paper and generating their corresponding plots.

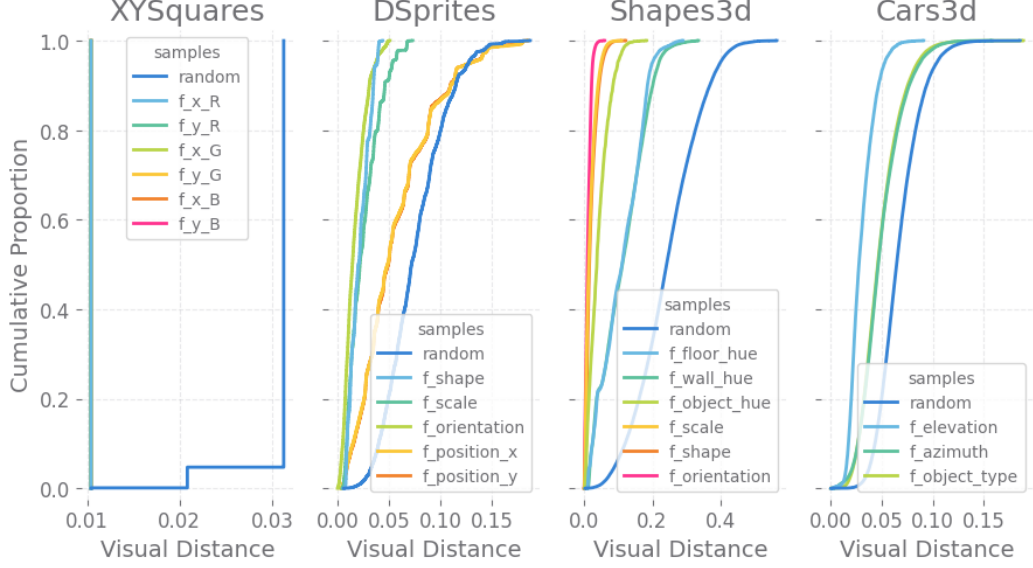


Figure 12. Cumulative proportion of visual distance values between pairs sampled along factor traversals, compared to visual distances between random pairs. Factors which are more important for the VAE to learn first to minimise the reconstruction loss have higher average visual distances (lines shifted further to the right). This corresponds to the experimental results from Burgess et al. [2] which show that as the information capacity of a VAE is increased, it learns factors in order. For dSprites, this is x and y position, followed by scale, then shape, and finally orientation.

Dataset	Factor	Mean Dist.	Dist. Std.
Cars3D [24]	azimuth	0.0355	0.0185
	object type	0.0349	0.0176
	elevation	0.0174	0.0100
	random	0.0519	0.0188
3D Shapes [3]	wall hue	0.1122	0.0661
	floor hue	0.1086	0.0623
	object hue	0.0416	0.0292
	shape	0.0207	0.0161
	scale	0.0182	0.0153
Small NORB [16]	orientation	0.0116	0.0079
	random	0.2432	0.0918
	lighting	0.0531	0.0563
	category	0.0113	0.0066
dSprites [21]	rotation	0.0090	0.0071
	instance	0.0068	0.0048
	elevation	0.0034	0.0030
	random	0.0535	0.0529
	position y	0.0584	0.0378
XYSquares	position x	0.0559	0.0363
	scale	0.0250	0.0148
	shape	0.0214	0.0095
	orientation	0.0172	0.0106
	random	0.0754	0.0289
XYSquares	y (B)	0.0104	0.0000
	x (B)	0.0104	0.0000
	y (G)	0.0104	0.0000
	x (G)	0.0104	0.0000
	y (R)	0.0104	0.0000
	x (R)	0.0104	0.0000
	random	0.0308	0.0022

Table 4. Average visual distances sampled between observation pairs taken along random factor traversals. Factors are sorted in order of importance. Factors listed first have higher visual distances on average and should be prioritised by the model. For comparison, the average distance between any random pair in the dataset is given. The average distances between pairs along factor traversals are usually less than the random distance, indicating that the ground-truth factors correspond to axes in the data. Averages are taken over 50000 random pairs.